Automatic Region Segmentation for High-resolution Palmprint Recognition: Towards Forensic Scenarios

Ruifang Wang, Daniel Ramos, Julian Fierrez and Ram P. Krish
ATVS - Biometric Recognition Group, Escuela Politecnica Superior (EPS)
Universidad Autonoma de Madrid (UAM)
Francisco Tomas y Valiente 11, 28049 Madrid, Spain
Email: {ruifang.wang, daniel.ramos, julian.fierrez, ram.krish}@uam.es

***Abstract*—Recently, a novel matching strategy based on regional fusion for high resolution palmprint recognition arises for both forensic and civil applications, under the concept of different regional discriminability of three palm regions, i.e., interdigital, hypothenar and thenar. This matching strategy requires accurate automatic region segmentation techniques since manual region segmentation is time consuming. In this work, we develop automatic region segmentation techniques based on datum point detection for high-resolution palmprint recognition which can be further applied to forensic applications. Firstly, Canny edge detector is applied to a full palmprint to obtain gradient magnitudes and strong edges. Then a first datum point, i.e., the endpoint of heart line, is detected by using convex hull on gradient magnitude image and its left/right differential image and strong edge image. A second datum point, i.e., the endpoint of life line, is estimated based on the position and direction of the first datum point and statistical average distance between the two datum points. Finally, segmented palm regions are generated based on the two datum points and their perpendicular bisector. To evaluate the accuracy of our region segmentation method, we compare the automatic segmentation with manual segmentation performed on a public high resolution palmprint database THUPALMLAB with full palmprint images. The regional error rates of interdigital, thenar and hypothenar regions are 15.72%, 17.05% and 21.38% respectively. And the total error rate is 19.54% relative to full palmprint images.**

I. Introduction

Recently, high resolution palmprint recognition has aroused research highlights due to the availability of live-scan palmprint technology and significant attention in forensic and civil applications. Since it deals with palmprints captured at 500 dpi at least, rich types of features, such as minutiae, principal lines, and even pores, can be used for high-resolution palmprint matching. Depending on the application fields, two kinds of matching strategy have been developed essentially following the minutiae-based matching methods, i.e., full-to-full palmprint comparison [1]–[3] for civil applications and partial-to-full/latent-to-full palmprint comparison [4]–[7] for forensic applications. As argued in the most recent work on forensic palmprint recognition [6], full-to-full palmprint matching algorithms would face problems when they are applied to forensic palmprint recognition where latent marks have much smaller area than full palmprints. As a first step towards improving the performance of high-resolution palmprint recognition for forensic scenarios, a novel two-stage matching strategy [8] arises recently. It includes, 1) region-to-region palmprint comparison; 2) regional fusion at score level. This is motivated by the finding that the three palm regions divided by three major creases as shown in Figure 1, i.e., interdigital, hypothenar and thenar, have different performance according to matching accuracy, as indicated in [5].

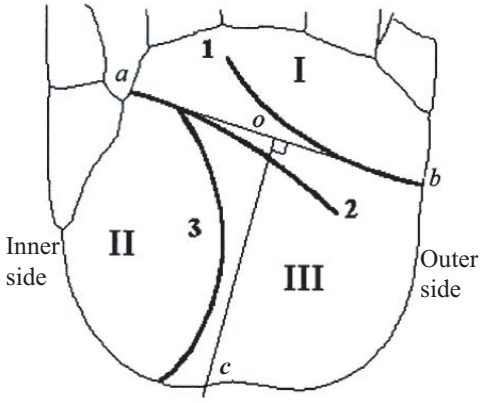

Fig. 1. Definitions of a palmprint: principal lines (1 - heart line, 2 - head line and 3 - life line), palmprint regions (I - interdigital region, II - thenar region and III - hypothenar region) and datum points (a, b-endpoint, o-their midpoint) [9]. c is the intersection point of the bottom boundary of a palm and the perpendicular bisector of the line segment $\overline{ab}$. Here $\overline{ab}$ and $\overline{oc}$ are used for region segmentation.

This matching strategy requires accurate automatic region segmentation techniques. Therefore, in this work, we develop automatic region segmentation techniques for high-resolution palmprint recognition which can be further applied to forensic applications. We propose an automatic region segmentation method based on datum points (see Figure 1) defined in [9] which remain stable according to their locations on principal lines in a full palmprint. Firstly, Canny edge detector [10] is applied to a full palmprint to obtain gradient magnitudes and strong edges. Then a first datum point, i.e., the endpoint of heart line, is detected by using convex hull [11] on gradient magnitude image and its left/right differential image and strong edge image. A second datum point, i.e., the endpoint of life line, is estimated based on the position of the first datum point and statistical average distance between the two datum points. Finally, segmented palm regions are generated based on the two datum points and their perpendicular bisector.

To evaluate the accuracy of our region segmentation method, we compare the automatic segmentation with manual segmentation (see one example in Figure 2) performed on a public high resolution palmprint database THUPALMLAB

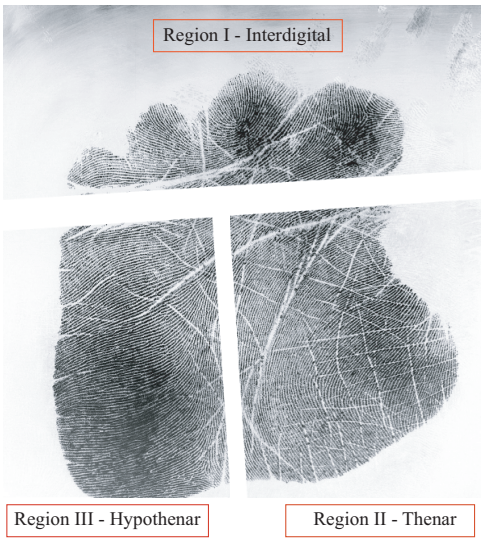

Fig. 2. Manually segmented regions for a sample palmprint.

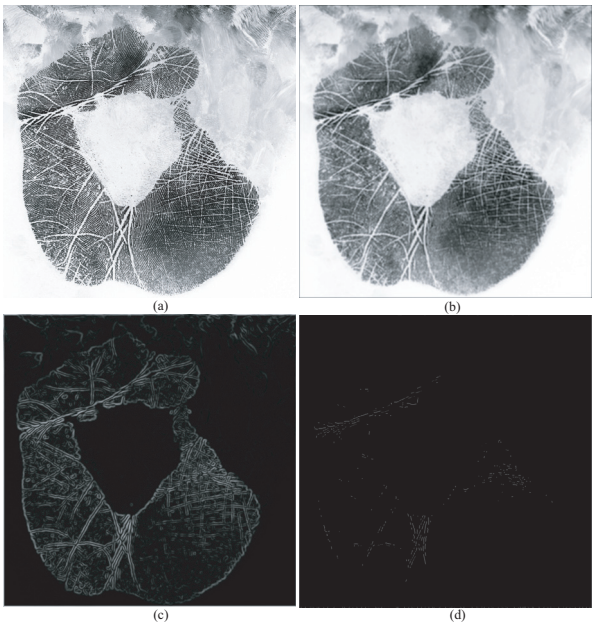

Fig. 3. Canny edge detection for a sample palmprint. (a) Input image, (b) smoothed image, (c) gradient magnitudes (I_G), (d) final strong edges detected (I_E).

[12] with full palmprint images with size of 2040 $\times$ 2040 pixels. Two types of errors, i.e., regional error and total error, are defined by counting the number of different pixels between two regions to measure segmentation performance. The regional error rates of interdigital, thenar and hypothenar regions are 15.72%, 17.05% and 21.38% respectively. And the total error rate is 19.54% relative to full palmprint images. The results show that the proposed automatic region segmentation method performs fairly well at pixel level considering the large image size and can be further used in regional fusion for high-resolution palmprint recognition especially for forensic applications.

The rest of the paper is organized as follows. Section II describes our proposed automatic region segmentation method. Section III shows experimental results on performance of the segmentation method. Finally, conclusions are given in Section IV.

II. Automatic Region Segmentation of Palmprints

In this section, we describe our proposed automatic region segmentation method based on datum points for high-resolution palmprints. It includes three stages: 1) edge detection, 2) datum point detection, and 3) region generation. Recalling the typical process of capturing high-resolution palmprints, e.g., inked images for forensic scenarios, we found that the outer side of a full palm can be captured more completely compared to the inner side due to the property of palm geometry under pressure. It means that the outer side of a palm can be placed flat easier than the inner side. In a practical way, this finding inspires us to focus on first detecting the datum point b on the outer side and then estimating another datum point a on the inner side as shown in Figure 1.

A. Canny Edge Detection for Palmprints

The purpose of edge detection in general is to significantly reduce the amount of data in an image, while preserving the structural properties to be used for further image processing. In our research, we need to preserve strong edges in palmprints, i.e., principal lines and contour lines for the next-stage processing since datum points are normally located on those strong edges. To this purpose, we use Canny edge detector [10] for palmprint edge detection as it has become one of the standard edge detection methods still used in research commonly.

Generally, the Canny edge detection algorithm runs five steps as follows.

- Step 1: **Smoothing**. To remove noise, Gaussian filter with the form in Equations (1) and (2) is used for blurring the image.

$$h(n_1, n_2) = \frac{h_g(n_1, n_2)}{\sum_{n_1=1}^{N_1} \sum_{n_2=1}^{N_2} h_g(n_1, n_2)}, \quad (1)$$

$$h_g(n_1, n_2) = e^{\frac{-({n_1}^2 + {n_2}^2)}{2\sigma^2}}, \quad (2)$$

  where N_1 and N_2 denote the filter size in width and height, and σ is the standard deviation. In our experiments, the filter size $N_1 = N_2 = 15$ and standard deviation $\sigma = 8$ are chosen empirically for palmprints. The effect of smoothing a sample palmprint with the filter is shown in Figure 3 (b).

- Step 2: **Finding gradients**. By calculating gradients at each pixel in the smoothed image in the x- and y-direction respectively, the gradient magnitudes $|G|$ (also known as the $edge\ strengths$) can then be determined as an Euclidean distance measure by applying the law of Pythagoras as shown in Equation (3), and the directions θ are calculated using Equation (4). The initial edges should be marked where the gradients of the image has large magnitudes as shown in Figure 3 (c).

$$|G| = \sqrt{{G_x}^2 + {G_y}^2}, \quad (3)$$

$$\theta = \arctan(\frac{|G_x|}{|G_y|}), \tag{4}$$

where G_x and G_y are the gradients in the x- and y-directions respectively.

- Step 3: **Non-maximum suppression**. In this step, the blurred edges in the image of gradient magnitudes (see Figure 3 (c)) are converted to sharp edges. Basically this is done by preserving all local maxima in the gradient image, and setting other pixels to black pixels, i.e., pixel value = 0. To determine all local maxima, an 8-connected neighbourhood is used for each pixel in the gradient image.

- Step 4: **Double thresholding**. Potential edges are determined by two thresholds, i.e., a low threshold λ_l and a high threshold λ_h calculated by

$$\lambda_l = C_l \cdot \max(|G|), \tag{5}$$

$$\lambda_h = C_h \cdot \max(|G|), \tag{6}$$

where C_l and C_h are two factors with empirical values 0.1 and 0.4 respectively. Edge pixels stronger than the high threshold are marked as $strong$; edge pixels weaker than the low threshold are suppressed and edge pixels between the two thresholds are marked as $weak$.

- Step 5: **Edge tracking**. Final edges are determined by suppressing all edges that are not connected to a very certain (strong) edge, as shown in Figure 3 (d).

The source code of Canny edge detector we used can be found in [13]. And the images in this section are generated using the code.

B. Datum Point Detection Based on Convex Hull Comparison

It is interesting that the datum point b and contour line on the outer side of a palm appear on both the gradient magnitude image I_G (see Figure 3 (c)) and the final edge image I_E (see Figure 3 (d)). However, the convex hulls of strong pixels in the two images can be different due to much less details in the edge image. Inspired by this finding, we propose a novel method of datum point detection based on convex hull comparison. It contains three steps as described below.

1) Single thresholding of gradient magnitudes: This step is to remove background noise in the gradient magnitude image as preparation for convex hull comparison. In the image I_G, pixels with gradient magnitude values smaller than a threshold g_0 (set to 1.8 empirically) are set to black pixels while pixels with large gradient magnitude values are preserved with original values. In this way, we generate a new image of gradient magnitudes I_{G_0} as shown in Figure 4 (a). Then starting from the image I_{G_0}, We generate a left differential image I_{G_l} with a threshold g_l of gradient magnitude value with a differential step of t pixels for a left palm image, and a right differential image I_{G_r} with a threshold g_r for a right palm image. The two images are defined below.

$$I_{G_l}(i,j) = \begin{cases} I_{G_0}(i,j), if\ I_{G_0}(i,j) - I_{G_0}(i,j-t) > g_l \\ 0, \qquad if\ I_{G_0}(i,j) - I_{G_0}(i,j-t) \leqslant g_l \end{cases} \tag{7}$$

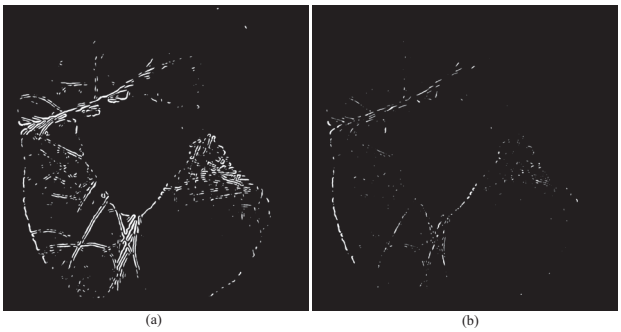

Fig. 4. Thresholding of gradient magnitudes. (a) Gradient magnitude image after thresholding (I_{G_0}), (b) Left differential image after thresholding (I_{G_l}).

$$I_{G_r}(i,j) = \begin{cases} I_{G_0}(i,j), if\ I_{G_0}(i,j+t) - I_{G_0}(i,j) > g_r \\ 0, \qquad if\ I_{G_0}(i,j+t) - I_{G_0}(i,j) \leqslant g_r \end{cases} \tag{8}$$

Here we choose the differential step $t = 20$ after observing the ridge width in the palmprints. Both thresholds g_l and g_r are close to g_0 in order to preserve the details of contour line on the outer side of a palm where the datum point b exists, and their empirical values are 1.7 and 1.6 respectively. Taking the left palm image used in Section II-A as an example, we show its gradient magnitude image after thresholding and left differential image after thresholding in Figure 4.

2) Detecting the datum point b: Given two images I_{G_0} and I_E, two sets of initial contour points P_G and P_E are generated by selecting 2 boarder pixels in each row (i.e., left most and right most grey pixels) and 2 boarder pixels in each column (i.e., top most and bottom most grey pixels). Then convex hulls of P_G and P_E are generated and represented by two sets of final contour points, i.e., $K_G \subseteq P_G$ and $K_E \subseteq P_E$ respectively. Comparison between the contour points K_G and K_E are performed, and candidates of datum point b are selected as K_{G_b} by the following rule:

$$K_{G_b} = \{p : \forall_{p \in K_G} \forall_{p' \in K_E} [\mathfrak{D}(p,p') \leq D_0]\}, \tag{9}$$

where $\mathfrak{D}(p,p')$ is the Euclidean distance between two pixels p and p', and the threshold D_0 is 12 pixels empirically. Finally, the datum point candidate b_e is located at the most upper-left point in K_{G_b} with the direction assigned by the line segment from the candidate to the secondary most upper-left point for a left palm image, or the most upper-right point with the direction assigned by the line segment from the candidate to the secondary most upper-right point for a right palm image. Similarly, we perform convex hull comparison between the two images I_{G_0} and I_{G_l} for a left palm image or I_{G_r} for a right palm image, to locate another candidate b_l or b_r. For a left palm image, the detected candidates of datum point b are shown in Figure 5 (a) and (b).

3) Estimating the datum point a: For each candidate of datum point b detected in Step 2, we estimate the position of its corresponding candidate of datum point a according to the following rules: (1) The direction of a is perpendicular to the direction of b; (2) a is on the right side of b for a left palm image, and on the left side of b for a right palm image; (3) the distance between b and a falls in a relatively small range and then an average value of the distance can be used.

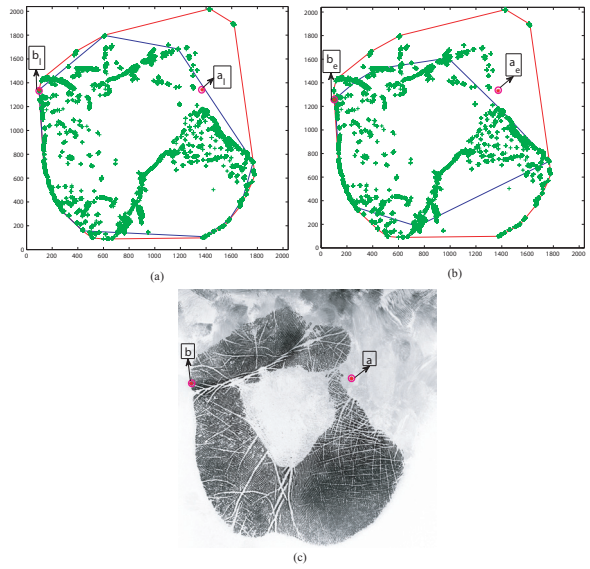

Fig. 5. Detected datum points by using convex hull. (a) Convex hull on I_{G_0} and I_{G_l}, (b) convex hull on I_{G_0} and I_E, (c) final datum points a and b.

In our experiments, we use a statistical average value of 1272 in pixel as the length of $\overline{ab}$ estimated from manual selected datum points on the palmprint database THUPALMLAB. After applying the above rules, two candidates a_e and a_l or a_r can be located. The final datum points a and b are determined as the midpoints of $\overline{a_e a_l}$ and $\overline{b_e b_l}$ for a left palm or the midpoints of $\overline{a_e a_r}$ and $\overline{b_e b_r}$ for a right palm. For a left palm image, the detected candidates of datum point a are shown in Figure 5 (a) and (b), and the final detected datum points a and b are shown in Figure 5 (c).

C. Region Generation Using Datum Points

After datum points a and b are located, a palm can be divided into three regions, including interdigital region (I), thenar region (II) and hypothenar region (III) by the connections between the endpoints and their perpendicular bisector, i.e., line segments $\overline{ab}$ and $\overline{oc}$ as shown in Figure 1. Firstly, we calculate the position of the midpoint o of line segment $\overline{ab}$. Then the endpoint c is located as the intersection of the perpendicular bisector of $\overline{ab}$ and the bottom boundary of the palmprint in most cases. Due to pose effect when capturing palmprints under pressure, the endpoint c can also locate on the bottom part of left/right boundary. Finally we divide each palmprint into those three regions by treating the line segments $\overline{ab}$ and $\overline{oc}$ as boundary lines.

III. Experiments

A. Palmprint Database

We evaluate our automatic region segmentation method compared to manual segmentation on a public high-resolution palmprint database, THUPALMLAB [12]. The whole database contains 1280 full palmprints from 160 palms, i.e., 80 subjects with left and right palms, and 8 impressions captured from each palm with a resolution of 500 ppi and image size of 2040×2040 pixels. In our experiments, we use a subset from THUPALMLAB for evaluation, including palmprints from the last 50 subjects, i.e., $50 \times 2 \times 8 = 800$ palmprint images.

On the subset database, we execute manual segmentation. Firstly, we manually choose endpoints a and b according to their definition and obtain their position with X and Y axis values. Then the positions of points o and c are calculated. Finally, three regions are obtained in the same way as that for automatically segmented regions.

B. Measures of Segmentation Error

It is important to define the segmentation error to measure the accuracy of segmentation algorithms. As indicated in [14], two types of errors should be considered, i.e., Under Detection Measure (UDM) and Over Detection Measure (ODM). Let R_A be the automatically segmented region (resulting region), and R_M the corresponding manually segmented region (reference region). The discrepancy that may exist between the two regions is induced by:

- The under detected pixels which are pixels that belong to the manually segmented region and not belong to the automatically segmented region.
- The over detected pixels which are pixels that belong to the automatically segmented region and not belong to the manually segmented region.

We are measuring discrepancies among automatically segmented and manually segmented regions, and those discrepancies are related in the three regions for each palmprint. Therefore, we will not separate Under Detection Measure and Over Detection Measure. Instead, for each region, we sum up the pixels both under detected and over detected to define a measure for regional segmentation error which is calculated as following,

$$e_{_R} = \frac{N_D}{N_R}, \tag{10}$$

where N_D is the number of different pixels (both under detected and over detected) between two corresponding regions, i.e., one segmented automatically and the other segmented manually, and N_R is the total number of pixels in the manually segmented region. Figure 6 shows the error pixels for one automatically segmented region compared to its corresponding manually segmented region.

For a full palmprint, we also define a measure for total segmentation error which is calculated as following,

$$e_{_F} = \frac{\sum_{i=1}^{3} N_{D_i}}{N_F}, \tag{11}$$

where N_{D_i} is the number of different pixels for each region, i = 1, 2, 3, corresponding to Region I, II, III respectively. N_F is the total number of pixels in the original full palmprint, simply determined by the full image size. In our experiments, $N_F = 2040 \times 2040$.

Finally, evaluating on a database, we will get 3 regional error rates represented by the average values of $e_{_R}$s from all palmprints in each of the three regions respectively. Similarly, we will also get one total error rate represented by the average value of $e_{_F}$s from all palmprints.

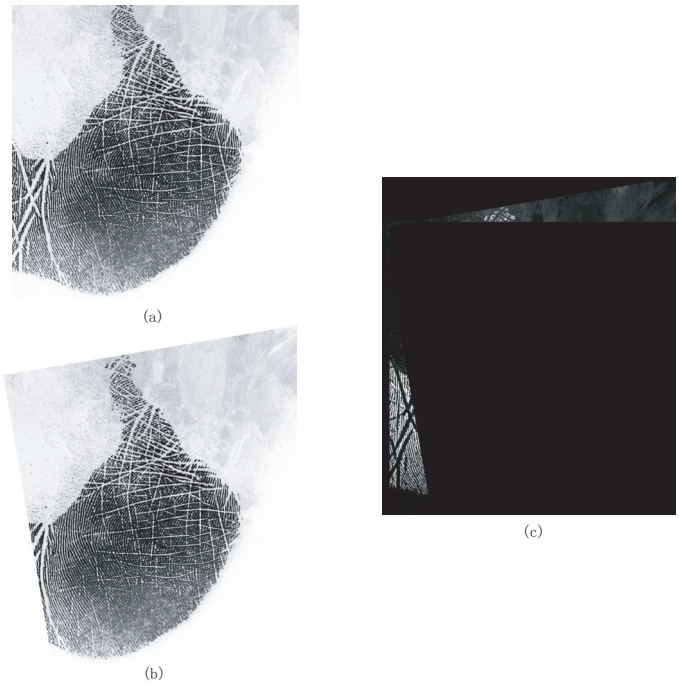

Fig. 6. Regional segmentation error. (a) Automatically segmented region, (b) manually segmented region, (c) error area.

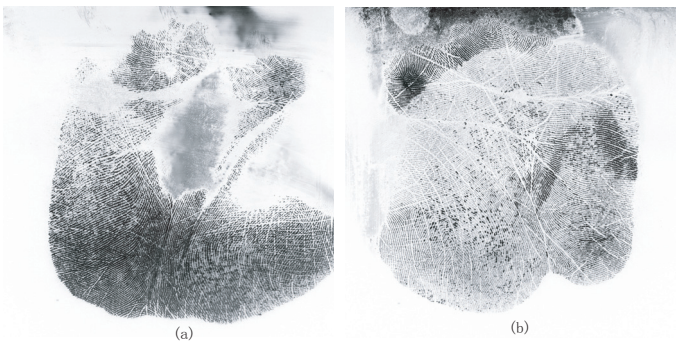

Fig. 7. Sample images where datum point b was not detected. (a) A sample image without datum point b from Subset B, (b) A failed image with datum point b from Subset A.

C. Results

As our automatic segmentation method mainly works by assuming that datum point b exists in the palmprint, we first divide the database into two categories, i.e., Subset A with datum point b and Subset B without datum point b (see one sample image in Figure 7 (a)), and count the number of images on each subset. Then in Subset A, we also count the number of failed images (see one sample image in Figure 7 (b)) due to low image quality which means bad contrast between the palm region and the background. The categories are shown in Table 1.

Using the successful images in Subset A, we obtained results regarding regional segmentation error and total segmentation error as shown in Table 2. The regional error rates of interdigital (I), thenar (II) and hypothenar (III) regions are 15.72%, 17.05% and 21.38% respectively. And the total error rate is 19.54% relative to full palmprint images.

TABLE I. THE CATEGORIES OF THE SUB-DATABASE FROM THUPALMLAB.

Categories		Number of palmprints
Subset A	Successful detection of b	702
	Failed detection of b	28
Subset B		70

TABLE II. ERROR RATES OF AUTOMATIC REGION SEGMENTATION COMPARED TO MANUAL SEGMENTATION ON SUBSET A.

Region	Regional error rate	Total error rate
Interdigital (I)	15.72%	19.54%
Thenar (II)	17.05%	
Hypothenar (III)	21.38%	

IV. CONCLUSION

In this work, we proposed an automatic region segmentation method based on datum point detection for high-resolution palmprint recognition which can be further applied to forensic applications. Firstly, we used Canny edge detector to obtain gradient magnitudes and strong edges in a full palmprint. Then a first datum point, i.e., the endpoint of heart line, is detected by using convex hull comparison on gradient magnitude image and its left/right differential image and strong edge image. A second datum point, i.e., the endpoint of life line, is estimated based on the position and direction of the first datum point and statistical average distance between the two datum points. Finally, segmented palm regions are generated based on the two datum points and their perpendicular bisector. This procedure requires prior knowledge of the palm order, i.e., left or right hand, which is available in forensic databases typically. To evaluate the accuracy of our region segmentation method, we compare the automatic segmentation with manual segmentation performed on a public high resolution palmprint database THUPALMLAB with full palmprint images. The regional error rates of interdigital, thenar and hypothenar regions are 15.72%, 17.05% and 21.38% respectively, and the total error rate is 19.54% relative to full palmprint images. The results show that the proposed automatic region segmentation method performs fairly well at pixel level and can be further used in regional fusion for high-resolution palmprint recognition especially for forensic applications.

To further improve automatic region segmentation, we will try to combine convex hull comparison results using all left, right, up and down differential images for gradient magnitudes. And we will deal with palmprint images where datum point b does not exist.

ACKNOWLEDGMENT

R. Wang and R. Krish are supported by Marie Curie Fellowships under project BBfor2 (FP7-ITN-238803). This work has also been partially supported by Spanish Guardia Civil, "Cátedra UAM-Telefónica", and projects Bio-Shield (TEC2012-34881) and Contexts (S2009/TIC-1485).

REFERENCES

[1] J. Dai and J. Zhou, "Multifeature-based high-resolution palmprint recognition," *IEEE Trans. Pattern Anal. Mach. Intell.*, vol. 33, no. 5, pp. 945–957, 2011.

[2] J. Dai, J. Feng, and J. Zhou, "Robust and efficient ridge-based palmprint matching," *IEEE Trans. Pattern Anal. Mach. Intell.*, vol. 34, no. 8, pp. 1618–1632, 2012.

[3] R. Cappelli, M. Ferrara, and D. Maio, "A fast and accurate palmprint recognition system based on minutiae," *IEEE Trans. Syst., Man, Cybern. B*, vol. 42, no. 3, pp. 956–962, 2012.

[4] A. Jain and M. Demirkus, "On latent palmprint matching," Michigan State University, MI, Tech. Rep. MSU-CSE-08.8.2008, May 2008.

[5] A. Jain and J. Feng, "Latent palmprint matching," *IEEE Trans. Pattern Anal. Mach. Intell.*, vol. 31, no. 6, pp. 1032–1047, 2009.

[6] E. Liu, A. K. Jain, and J. Tian, "A coarse to fine minutiae-based latent palmprint matching," IEEE Trans. Pattern Anal. Mach. Intell., 2013, to be published.

[7] R. Wang, D. Ramos, and J. Fierrez, "Improving radial triangulation-based forensic palmprint recognition according to point pattern comparison by relaxation," in *Proc. IAPR/IEEE International Conference on Biometrics (ICB)*, New Delhi, India, Mar. 2012, pp. 427–432.

[8] R. Wang, D. Ramos, J. Fierrez, and R. Krish, "Towards regional fusion for high-resolution palmprint recognition," XXVI SIBGRAPI Conference on Grapghic Patterns and Images, Arequipa, Peru, August 2013, to be published.

[9] D. Zhang and W. Shu, "Two novel characteristics in palmprint verification: Datum point invariance and line feature matching," *Pattern Recognition*, vol. 32, no. 4, pp. 691–702, 1999.

[10] J. Canny, "A computational approach to edge detection," *IEEE Trans. Pattern Anal. Mach. Intell.*, vol. 8, no. 6, pp. 679–698, 1986.

[11] E. W. Weisstein. (2007) Convex hull. [Online]. Available: http://mathworld.wolfram.com/ConvexHull.html

[12] (2011) Thupalmlab palmprint database. [Online]. Available: http://ivg.au.tsinghua.edu.cn/index.php?n=Data.Tsinghua500ppi

[13] A. Senapati. (2011) Canny edge detector. [Online]. Available: http://www.mathworks.com/matlabcentral/fileexchange/34231-canny-edge-detection/content/canny.m

[14] A. Goumeidane and M. Khamadja, "Error measures for segmentation results: Evaluation on synthetic images," in *Proc. IEEE International Conference on Electronics, Circuits, and Systems (ICECS)*, Athens, Greece, Dec. 2010, pp. 158–161.